CELT Tech Note No. 11

Sensor Noise Propagation for CELT: Control Algorithm Analysis

D. MacMartin
8/31/01

One of the contributions to the telescope error budget associated with the active degrees of freedom of the primary mirror is˚sensor noise propagation. This source can become significant because primary mirror deflections of low spatial wavenumber are almost unobservable with segment edge sensors; as a result, the current plan is to also incorporate wavefront sensing for the primary mirror control. The resulting contribution to the error budget depends on the control algorithm, and the control bandwidth in particular. Because it may be useful to increase the control bandwidth beyond that used on Keck in order to compensate for the wind, this dependence of sensor noise on bandwidth must be understood. This note, therefore, clarifies the current estimated contributions to the telescope error budget associated with sensor noise propagation through the primary mirror active control system, taking into account: (i)˚the active control bandwidth, (ii)˚the combination of wavefront and edge sensor information, and (iii)˚the conversion of the resulting error into a seeing-limited specification. Error propagation, as expected, is not a driver for diffraction-limited observations.

The sensor noise propagation is discussed in references 1, 2 and 3.

1. Existing algorithm & analysis

Some definitions and analysis are necessary for background; the following is from Ref. 3.

Each segment of the primary mirror has three out of plane degrees of freedom, and it is convenient to use the displacement at each of the actuator locations to describe the position of each segment. Thus the overall deformation of the primary mirror can be determined from the vector x of segment deflections at the actuator locations. The rms surface error of the primary mirror is S_{rms}˚=˚$1.06\cdot\sigma_x$ (based purely on geometry), where σ_x is the rms of the vector x, and the rms wavefront error is double the rms surface error. The contribution to enclosed energy on the sky, $\theta(80)$, is obtained by ray-tracing analysis; for a Gaussian point spread function and uncorrelated displacement errors σ_x, the result is given by $\theta(80)$˚=˚$1.27\cdot\theta_{rms}$˚=˚$11.5\cdot\sigma_x$ (this is specific to geometry choices such as the distance between actuators and the center of a segment). The derivation of the factors is documented in Ref.˚1. Note that for sensor noise propagation, the displacement errors are *not* uncorrelated, and this needs to be accounted for in the conversion to $\theta(80)$.

An initial analysis of the error propagation resulting from sensor noise is described in Ref.˚2. With only the capacitive edge sensors, the low wave-number (spatially smooth) modes have poor observability, and thus the computed actuator moves amplify the sensor noise. Including wavefront information improves the observability of these low wave-number modes. Note that the capacitive edge sensors described in Ref.˚4 measure the differential capacitance between an upper and lower capacitor, and are sensitive to both

vertical translation of neighboring segments, and to relative rotation about the axis defined by the segment edge. The first of these is much more significant, and at the time of writing Ref. 2, only the first was included. However, including the sensor response due to relative rotation between segments is significant because the focus mode becomes observable, and the low order modes also become slightly more observable. The results presented below include the rotational sensitivity on the edge sensors, and then add the impact of the wavefront sensors.

The vector of edge sensor readings y_e that result from segment displacements satisfies

$$y_e = A_e x + n_e$$

where the matrix A_e is determined from the geometry, and n_e is the edge sensor noise. The singular value decomposition of A_e motivates a useful set of basis functions for representing spatial deflection shapes of the mirror. With $A_e = U\Sigma V^T$, Σ a diagonal matrix of singular values σ_i, and U, V unitary, then $\xi = V^T x$ or $x = V\xi$ is a useful change of basis; the columns of V will be referred to as modes for convenience, and represent a complete orthonormal set which span the space of all possible configurations of the primary mirror. Large singular values of A_e correspond to highly observable deflection shapes, which are those with large deflections between neighboring segments for unit overall rms deflection. The matrix A_e has three singular values equal to zero, corresponding to overall rigid body deflection of the primary mirror. The focus mode (where every segment has the same dihedral angle between its neighbors) has zero relative edge displacement between segments, but is observable with the current sensor geometry.

The simplest control law is to estimate the deflections at the actuator locations as

$$\hat{x} = A^{\#} y,$$

and compute the desired change in the actuator commands u via

$$\Delta u = \beta x,$$

where $A^{\#}$ is the left pseudo-inverse $(A^T A)^{-1} A^T$ (readily computable from the singular value decomposition, $A^{\#}$ has singular values σ_i^{-1}) and $\beta<1$ determines the bandwidth. This is the feedback control law used at Keck. (Keck also has a feedforward term that accounts for the predictable gravity variation, but that term does not affect the analysis of either sensor noise or control bandwidth.) The estimate x is optimal if the noise on the sensors is small compared to the disturbances that the control is intended to correct. This results in a simpler problem formulation. This restriction will be removed later in this note. Note that separating the control law into two steps of estimating the errors at the actuator locations, and then correcting for them, simplifies the discussion both of the influence of the control gain, and of the inclusion of wavefront information.

With the integral control law above, deflections of any spatial shape are controlled with the same bandwidth. However, modes with small singular value in A have large singular values in $A^{\#}$, and hence the control law will amplify whatever sensor noise exists in these directions. Assuming white noise, then the overall noise propagation from rms sensor noise to rms errors in estimating the deflection at the actuator locations is given by

$$\sigma_{x\text{-}x} = (\bullet\ \sigma^{-2}/N_a)^{1/2}$$

This formulation results in the error propagation estimates previously documented for the CELT A-matrix; depending on geometry assumed, the error propagation is ~16-30 (compared with 4.4 for Keck).

2. Impact of Control Bandwidth

The resulting error in actuator positions depends on the control gain, β. The controller acts as a low-pass filter on the noise, and thus if the noise has a flat power spectral density, the resulting contribution to the error budget is proportional to the square root of the bandwidth (the variance being proportional to the bandwidth). For $\beta \cdot 1$ the total error contribution is given by $(\beta/2)\cdot\sigma_{x\text{-}x}$.

The propagation through the controller is clearer, and more useful, if stated in terms of the control bandwidth rather than the control gain, and also easier if one works with a continuous-time analysis (which is adequate if the control bandwidth is much lower than the sample rate). The integral control law from y to u is $K(s) = A^{\#}\cdot k/s$, where s is the Laplace variable and k is the gain (which is related to the discrete-time gain β). The system transfer function $G(s) = A$. The response from disturbances to the surface error x resulting from this is $1/(1+GK) = s/(s+k)$; as desired, the control law attenuates disturbances below the control bandwidth, set by k. The response from sensor noise to surface error x is $K/(1+GK) = A^{\#}\cdot 1/(s/k+1)$; this is a low-pass filter that passes sensor noise through to surface errors below the control bandwidth and attenuates higher frequency sensor noise. The factor $A^{\#}$ is accounted for previously through the error propagation to the estimated surface errors, however, the low-pass filter also needs to be accounted for.

For a signal n with uniform PSD Φ (variance per Hertz) passed through a low-pass filter with corner frequency k rad/sec to give signal u, then

$$\langle u^2\rangle = \int G^* G\cdot d\omega\cdot(\Phi/(2\pi)) = k\pi/2\cdot(\Phi/(2\pi)).$$

Thus for a bandwidth $f_0 = k/(2\pi)$ in Hertz, $\sigma_u = (f_0\cdot\pi/2\cdot\Phi)^{-}$. (The factor of $\pi/2$ larger than the control bandwidth in computing the variance accounts for the fact that there is a contribution to the output variance due to noise that is above the control bandwidth.)

3. Edge sensor noise

The Keck sensor noise level, quoted at 6 nm, is the rms noise at the input to the controller. This has already been passed through a low-pass anti-aliasing filter with corner frequency of $f_a = 0.2$ Hz before being sampled at 2 Hz. Thus to obtain the nominal PSD of the capacitive sensor noise, Φ, one would need to account for this filtering, giving 115 nm^2/Hz, or 11 nm/sqrt(Hz). Alternatively, the effect of the control bandwidth can be accounted for via the ratio $(f_0/f_a)^{-}$. Assuming that the sensor PSD is uniform with frequency, then this scale factor will be valid for $f_0 > f_a$ also. Of course, for larger control bandwidths, the actual anti-aliasing filter corner frequency and sensor sample rate would

need to be correspondingly increased; however, it is the control bandwidth that ultimately sets the contribution to the error budget, and not the sampling rate.

For Keck, therefore, with a control bandwidth of roughly 0.05˚Hz, the total contribution to the error budget due to sensor noise can be obtained as the product of the sensor noise at 0.2˚Hz, the error multiplier from the A matrix (or rather from $A^{\#}$), and a factor accounting for the ratio of the control bandwidth to the sensor filter:

$$\sigma_{rms}{}^{\circ} = {}^{\circ}(6^{\circ}\text{nm})(4.4\ \text{nm/nm})\cdot(0.05/0.2^{\circ}\text{Hz/Hz})^{-\circ} = {}^{\circ}13^{\circ}\text{nm}$$

Alternatively, one can use the PSD specification for the sensor:

$$\sigma_{rms}{}^{\circ} = (11^{\circ}\text{nm/sqrt(Hz)})\cdot(4.4\ \text{nm/nm})\cdot((\pi/2)\cdot 0.05\text{Hz})^{-\circ}$$

The specification for the edge sensors for CELT is that they should have no more noise than those at Keck. Note that rather than specifying 6˚nm noise when passed through a filter with a 0.2˚Hz bandwidth, it would be preferable to specify the noise level as 11˚nm/sqrt(Hz). Also note that the source of the sensor noise at Keck is not fully understood, and therefore it may be possible to improve the noise levels for CELT. Conversely, the sensor geometry is different, and therefore it may be challenging to obtain comparable noise levels. The contribution to the error budget can again be computed from the rms sensor noise, the error multiplier from the A matrix, and the square root of the desired control bandwidth. Ignoring the focus mode, then the error multiplier is about 15 (α=0.10), hence for the same control bandwidth as Keck, the contribution to the error budget is about 50˚nm (surface error), while for a 1˚Hz bandwidth sufficient to compensate for some wind-induced deformation of the primary mirror, the contribution is about 200˚nm.

Of course, these need to be converted to contributions to $\theta(80)$ or uncorrectable wavefront error before determining whether there is a problem. Furthermore, wavefront information can be obtained for the lowest set of modes and used in conjunction with the edge sensors to provide improved estimates. Finally, if the reason for increasing the control bandwidth is to compensate for wind, then not every mode shape needs to have a higher bandwidth, since the wind is decorrelated over a distance of a few metres (see ref.˚5), hence there is no need to amplify the sensor noise of the poorly observed modes. Each of these will be dealt with in the subsequent sections.

4. Conversion to $\theta(80)$ errors

The contribution to image blur is obtained by considering the rms segment rotation for each mode. Denote the rms noise (from any source) on mode ξ_i as ζ_i. Thus for example with the control above, the residual noise on mode ξ_i is $\zeta_i{}^{\circ} = {}^{\circ}\mu\sigma_i^{-1}$, where μ is a constant that depends on the sensor noise and control bandwidth, and σ_i is the corresponding singular value of the A matrix. Furthermore, if the noise on each individual sensor is uncorrelated, then the noise on each mode is also uncorrelated. The image blur depends on the rms rotation, not on the rms displacement error *x*. For each mode, then, compute the multiplier *R* that is the ratio of rms rotation resulting from unit displacement in that mode. This can be done from geometry. The multiplier *R* is shown in Figure 1. The

high spatial wavelength modes result in larger rms rotation than the low wavenumber spatially smooth modes. (Note that the dip past mode 1000 is not an error; only the first ~1000 modes can truly be interpreted as smooth modes of a circular disc, and the remaining ~2000 modes are dominated by individual segment motions.)

The mean-square rotation due to the noise ζ on each mode is therefore $\sum(R_i^2\zeta_i^2)$; this is plotted in Figure 2. Combining the modal error multiplier with the modal rotation yields an error multiplier for CELT edge sensors of roughly 1.4˚mas/nm. This is the noise propagation factor from sensor noise to estimation errors in segment rotations, analogous to the earlier noise propagation from sensor noise to estimation errors in segment displacements. To obtain the contribution to the error budget, this factor needs to be combined with the sensor noise (11˚nm/sqrt(Hz)) and the control bandwidth (e.g. 0.05˚Hz or 1˚Hz) and the conversion factor from segment tips and tilts to $\theta(80)$ of 1.27. Thus with edge sensors alone, the two bandwidths would result in $\theta(80)$˚~˚5 or 25 mas respectively.

5. Diffraction-limited errors

With adaptive optics on, most of the errors introduced by sensor noise can be corrected. The errors that remain result from edge discontinuities between segments. A rough estimate for these can be obtained by noting that each inter-segment edge has two edge sensors, so that the resulting uncertainty in the edge discontinuity is $1/\mathrm{sqrt}(2)\cdot\Phi$. The uncertainty within the control bandwidth again scales with $((\pi/2)\cdot f_0)^{-}$.

The fraction of the rms edge discontinuity remaining after correction by adaptive optics is approximated by a 2-dimensional geometric argument. If the DM slopes were piecewise constant, then the residual displacement can be obtained from the ratio l/L where l is the length between DM actuators and L is the segment length. Integrating the area under the remaining triangle gives the controlled rms surface error σ_{ctrl} in terms of the uncontrolled rms error σ_{unc} as:

$$\sigma_{ctrl} = (l/L/12)\sigma_{unc}$$

For a deformable mirror with ~7000 actuators and a primary mirror with 1080 segments, l/L is ~2.5 hence $\sigma_{ctrl} \approx 0.18\sigma_{unc}$.

The residual wave-front error resulting from sensor noise propagation is therefore given by the product of all of these factors:

$$\sigma_{wf} = 2(0.18 \text{ nm ctrl/nm unctrl})\cdot(11 \text{ nm/sqrt(Hz)})\cdot(1/\mathrm{sqrt}(2))\cdot((\pi/2)\cdot f_0)^{-}$$

Thus for control bandwidths of 0.05 or 1˚Hz, the wavefront error will be 1 or 3.5˚nm. Wavefront information will not change this result significantly. This rough analysis verifies that sensor noise propagation is not a critical issue for diffraction-limited observations.

6. Inclusion of wavefront information

The displacement estimates for the low wave-number modes can be improved using optical wavefront information. A Shack-Hartmann wavefront sensor measures the average wavefront tip and tilt on each element of an array of lenslets. The corresponding sensor influence matrix A_w is computed by averaging the tip/tilt errors of the segments that are mapped onto each lenslet.

Since the wavefront information must be available anywhere in the sky, sufficient information must be obtainable from an 18.5 magnitude star. For a 90 lenslet array with realistic read noise, the sensor noise is roughly 30˚mas. This result is based on analysis by Chanan (this is documented in the first CELT quarterly report[6]), and corresponds to a 0.03˚s integration time. However, this estimate does *not* include the noise contribution from the atmosphere, which will be substantially larger. Without including this effect, the analysis can be considered illustrative, but not quantitatively accurate.

The edge and wavefront sensor information can then be combined to estimate the resulting error propagation. Figure 3 compares the modal error multipliers for the two different sensors, scaled by their respective noise levels, with modes ordered from lowest wave-number (least observable) to highest. Note that this figure was generated using a relative scale factor of 30˚mas to 6˚nm, which is not correct unless both values correspond to the same low-pass filtering. If the former number corresponds to a 33˚Hz update rate, then it could be passed through a 0.2˚Hz filter to give only 4˚mas of residual noise. (The factor to obtain the residual noise variance is the filter frequency with the same factor of $\pi/2$ from before, divided by the Nyquist rate for the unfiltered signal.) One could undoubtedly re-optimize the wavefront sensor for a lower output rate, the purpose of this is only to estimate the scaling between the two sensors of ~0.7˚mas/nm.

Even with the original scale factor in the figure of 5˚mas/nm, the wavefront sensor provides better information for the first 50 modes. The next section addresses combining the two sensors using a Kalman filter, however, for simplicity in our initial analysis we used the projection from the singular value decomposition of the edge sensor A matrix, and applied only wavefront information for the first 50 modes, and only edge sensor information for the remaining modes. With the scale factor of 5˚mas/nm, this gives a 6-fold reduction in the sensor noise error multiplier relative to using edge sensor information only. With the corrected scale factor of 0.7˚mas/nm, then the error multiplier drops down to 2.3 (with this noise, the wavefront information can be used for more than 50 modes, but the final error multiplier is not strongly sensitive to this).

The best approach is to use all of the information (wavefront and edge sensors) to estimate the entire displacement vector (represented either as errors at actuator locations, x, or as modes, ξ). Define a scaling parameter $\gamma^2 = \varphi_e/\varphi_w$, where φ_e and φ_w are the covariances associated with an individual edge sensor s and wavefront sensor s noise respectively. (It is assumed that the noise on each sensor of each type is uncorrelated and has the same covariance, so the covariance of n_e is $\Phi_e = \langle n_e n_e^T \rangle = \varphi_e I$ where the operator $\langle \cdot \rangle$ is the expectation, and I is the identity matrix of appropriate size. The scaling parameter γ is the ratio of rms sensor noise on the wavefront sensors relative to the edge

sensors, in appropriate units. An overall set of measurements $y^\circ = {}^\circ A x^\circ + {}^\circ n$ can then be created as the vector of y_e and γy_w, the corresponding matrix A formed by stacking A_e and γA_w, and a new estimate x° formed as before but using the pseudo-inverse of this new A matrix multiplying *all* of the sensor information. This estimate will be optimal for the combined set of sensors if the sensor noise is small compared to the disturbances. The singular values of this new A matrix give an improved noise multiplier compared to using one set of sensors for one set of modes and the other for the remainder; all sensors are used for all modes. The resulting curve is also plotted in the figure and, as expected, falls below either of the other curves. The noise multiplier obtained from the optimal combination of the sensors is about 7% better than the estimate of the noise multiplier obtained by using the wavefront information for the first 50 modes and the edge sensors for the remainder. That is, it is worth doing from the perspective of ultimately implementing the control, but does not substantially impact the assessment of error budgets. Also note that the value of γ used in creating the figure was again 5˚mas/nm, and thus the figure should be considered as a qualitative guide to the type of results one could expect, rather than a quantitative assessment. Thus the rms surface error is given by

$$\sigma_{rms} = (11^\circ \text{nm/sqrt(Hz)}) \cdot (2.1 \text{ nm/nm}) \cdot ((\pi/2) \cdot 0.05\text{Hz})^{-^\circ}$$

yielding 6 or 30˚nm rms surface error for a control bandwidth of 0.05 or 1˚Hz. While the wavefront error is considerable, most of it will be correctable by AO.

Figure 4 compares the wavefront and edge sensor information in terms of the error multipliers between sensor noise and rms segment rotation, a more useful figure of merit for the seeing-limited case. Again, this figure is plotted with $\gamma^\circ = 5^\circ$mas/nm. Adding the contributions from every mode gives the overall error multiplier as ~0.9 mas/nm, or roughly 2/3 of the value without wavefront information. For $\gamma^\circ = {}^\circ 0.7^\circ$mas/nm, the error multiplier only drops by about 10% to ~0.8˚mas/nm.

Comparisons can again be made as a function of control bandwidth:

$$\theta(80) = (11^\circ \text{nm/sqrt(Hz)}) \cdot (1.27\, \theta(80)/\theta_{rms}) \cdot (0.8 \text{ mas/nm}) \cdot ((\pi/2) \cdot 0.05\text{Hz})^{-^\circ}$$

giving $\theta(80) = 3^\circ$mas for a 0.05˚Hz bandwidth and $\theta(80) = 14^\circ$mas for a 1˚Hz bandwidth (compared with estimates of 5 and 25˚mas without the wavefront information).

Again, recall that the atmospheric contribution to the wavefront sensor has not been included, and the noise contribution will increase once this is taken into account.

7. Control algorithm notes

The current control algorithm (integral control based on the least-squares estimate $(A^T A)^{-1} A^T y$) is optimal if the sensor noise is small compared to disturbances, and yields the same bandwidth for every mode. However, if the control bandwidth is increased to compensate for wind-induced vibration, then the assumption of negligible sensor noise is no longer true. Due to the increased error propagation for CELT relative to Keck, negligible sensor noise may be a poor assumption even for the same control bandwidth. The optimal estimate of the position errors, and hence the optimal actuator commands,

can be obtained from a Kalman filter. The net effect is to make the bandwidth a function of the modal observability, so that there is greater filtering on those modes that are poorly estimated.

As above, define the combined vector of sensor measurements y and corresponding matrix A and noise n. Thus assume that the state vector x and measurement y satisfies:

$$x_{k+1} = Ax_k + u_k + w_k$$

$$y_k = Ax_k + n_k$$

Ignoring the control input u_k, then the estimate is given by the following equation, for some gain H.

$$\begin{aligned} \hat{x}_{k+1} &= \hat{x}_k + H(y_k - A\hat{x}_k) \\ &= (I - HA)\hat{x}_k + Hy_k \end{aligned}$$

Recall the singular value decomposition of $A = U\Sigma V^T$, with σ_i as the i^{th} singular value of A. Choose the matrix H to have the same structure as the pseudo-inverse of A, so that

$$H = V\Lambda U^T$$

where the modal gain matrix Λ has diagonal elements $\lambda_i = \sigma_i^{-1} F_i$ for some vector of modal factors F_i. With these definitions, then the estimate is a first order low-pass filter of the measurements, with a bandwidth that depends on the mode. If, for a given mode, $F_i = 1$, then the estimate for that mode is the same least squares estimate as before, and the resulting control law has the same bandwidth as before. For $F_i < 1$, then some additional filtering is done by the estimation and the control law $u_{k+1} = u_k - \hat{x}_k$ will have a lower bandwidth. (Note that the factor β has been removed, since any filtering can be done by the estimator, and it simplifies the discussion of the impact of F_i. If $\hat{x}_k$ is in fact the best possible estimate of the residual error at time step k, then there is no reason to further reduce the control gain; nonetheless it may still be a useful design parameter.)

The optimal value for H can be found through a Kalman filter. With the scaling γ on wavefront information, then the covariance $\Phi = \langle nn^T \rangle$ will be diagonal with elements φ_e (this assumption is not required, but simplifies the analysis). Define also the covariance matrix Θ of the noise w that represents the unpredictable component of the disturbances on the primary mirror (that is, after the predictable component of the gravity disturbance is removed through feedforward control). The optimal estimate minimizes the covariance Ξ of the estimation error, which is given by $e_k = \hat{x}_k - x_k$. The optimal gain is in general computed from the Discrete Algebraic Riccati equation. The matrices Ξ and H satisfy

$$\Psi - \Xi A^T (A\Xi A^T + \Phi)^{-1} A\Xi = 0$$

$$H = \Xi A^T (A\Xi A^T + \Phi)^{-1}$$

In the special case where the covariance matrices Ψ and Φ of w and n are diagonal with equal elements ψ and φ respectively, then H has the form $V\Lambda U^T$ written earlier, and λ_i

can be obtained from a scalar version of the equation for H and Ξ. The solution only depends on the ratio of the measurement and process noise, so define $\mu = \varphi/\psi$. Then

$$\lambda_i = \sigma_i^{-1} F_i,$$

$$F_i = \kappa_i \sigma_i^2 / (\kappa_i \sigma_i^2 + \mu)$$

$$\kappa_i = \frac{1}{2}(1 + (1 + 4\mu/\sigma_i^2)^{-\frac{1}{2}})$$

Thus for $\mu \to 0$ (no measurement noise), then the optimal gain matrix H is precisely the pseudo-inverse of A used earlier, and substituting this into the optimal estimator equation yields the optimal estimate used earlier that depends only on the current measurement. For $\mu \neq 0$, then the modal estimator gain is reduced by an amount dependent on the singular value of that mode; for well-observed modes (σ_i large), the factor remains close to unity.

The optimal estimator does precisely what one might expect. If every element of *x* is equally disturbed, and hence every mode ξ is equally disturbed (since the matrix V is unitary), then the estimates for those modes where the sensor information is reliable will be updated at a higher bandwidth than those modes where the sensor information is poor. These latter modes have a built in filter that averages out more of the information. The control law built on this estimator automatically controls the high spatial bandwidth modes at a higher temporal bandwidth than the poorly observed low spatial bandwidth modes. This is precisely the desired behaviour.

The approach above can be extended by including a proper model of the spatial scale of the disturbances (which would be modal; that is, the higher spatial frequency modes are more excited by disturbances such as wind than the lower spatial frequency modes). The control problem can similarly be solved in an optimal fashion. If all modes are weighted equally, then there is no change to the control law, but one could in principle also weight different modes based on their contribution to either a seeing-limited or AO performance metric. The resulting control law still uses all of the sensor information to compute each control signal, but in a modal manner. Alternatively, rather than pretending that we know the details of the disturbances and measurement noise processes, one can simply interpret the parameter μ above as a tuning parameter that gives us desirable control behaviour. The control bandwidth for the best observed modes can be increased without a significant increase in the sensor noise contribution to the error budget. Even a modest value of $\mu = 0.01$ yields a factor of 4 reduction in the error propagation using edge sensors only, for a constant bandwidth on the well observed modes. Conversely, the overall errors could be kept the same while the bandwidth of these well-observed modes is increased by a factor of 16.

8. Conclusions

A complete estimate of the propagation of sensor noise to errors in the actively controlled degrees of freedom of the primary mirror requires the control algorithm to be taken into account. In particular, the total contribution scales with the square root of the bandwidth

(the variance scales linearly). The control algorithm can be readily modified, with no increase in on-line computation, to allow the bandwidth to depend on the modal observability. This will allow the bandwidth of the high spatial wavenumber modes to be increased with less penalty on sensor noise propagation. A final estimate of the sensor noise propagation error will need to be done in conjunction with optimizing the control algorithm in order to trade the reduction in disturbances (e.g. wind-induced vibration) obtained with a higher bandwidth against the increase in sensor noise propagation.

The errors resulting from sensor noise are predominantly in the low wave-number modes that are poorly observed with edge sensors. Therefore, this is primarily a concern for seeing-limited, not diffraction-limited observations. Using the Keck edge sensor noise of 6˚nm with a 0.2˚Hz filter (or 11˚nm/sqrt(Hz)) and converting to θ(80) yields between 5 and 25˚mas noise for control bandwidths of 0.05 and 1 Hz respectively. (Even for the 1˚Hz bandwidth, the contribution to wavefront error with AO on is only 3.5˚nm.)

Including wavefront information has a significant impact on the residual surface errors due to sensor noise. The wavefront sensor noise has not yet been accurately estimated, as the (dominant) contribution from the atmosphere has not yet been accounted for. Nonetheless, an optimal combination of the two sensor systems is straightforward. Ignoring the atmospheric noise, the resulting contribution to θ(80) for control bandwidths of 0.05 and 1˚Hz is 3 or 14˚mas. Although it appears that it may be possible to meet the error budget without wavefront sensing, it seems prudent to continue to assume wavefront information in the design for two reasons; first because the design of the CELT edge sensors has not yet been completed and therefore the noise level is uncertain, and second, because the optimal control bandwidth to balance sensor noise propagation against residual higher frequency errors remains to be determined.

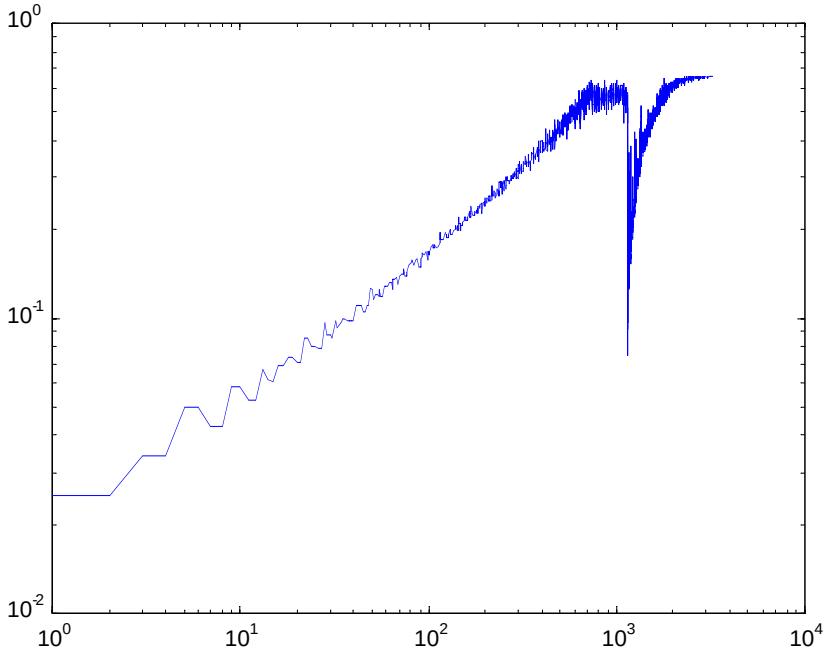

Figure 1. Ratio of rms tip/tilt of each mode to the rms displacement of each mode, in mas/nm. The low wavenumber, spatially smooth modes, have less rotation than piston. The last ~2000 modes involve individual segment rotations and are different in character.

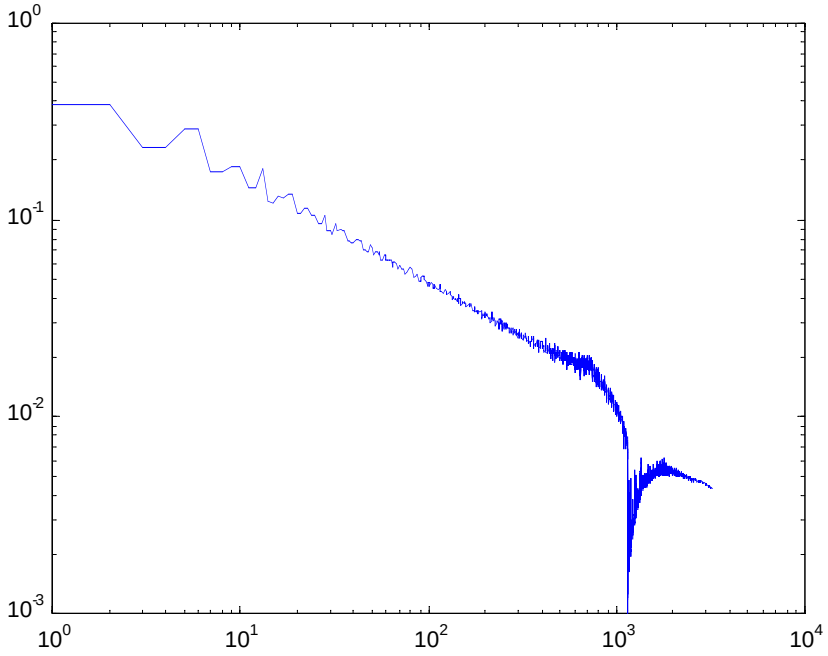

Figure 2. Modal error multipliers for seeing-limited case with edge sensors, in mas of segment rotation per nm of edge sensor noise.

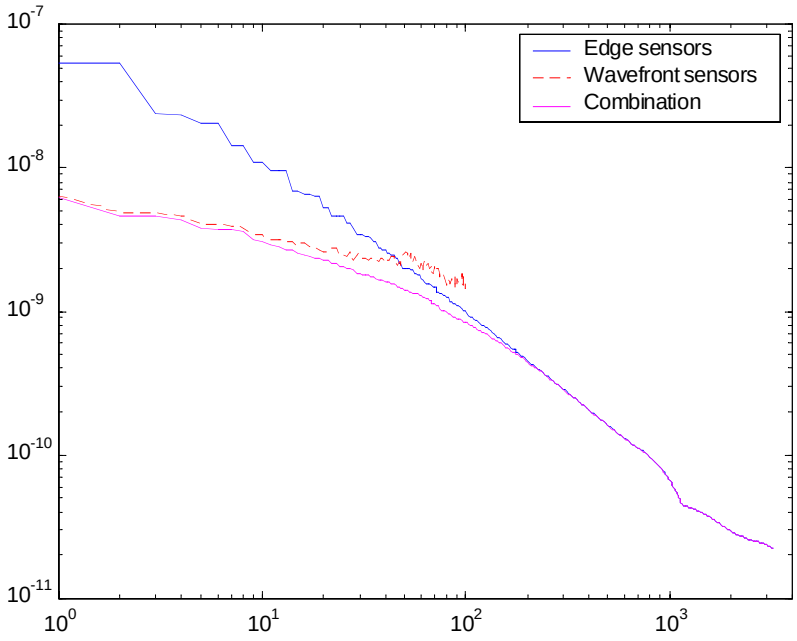

Figure 3. Qualitative comparison of CELT edge sensor and wavefront sensor modal error multipliers, and the error multiplier for the combined system. The relative factor between the two sensor systems (30mas/6nm) is perhaps a factor of 7 too high.

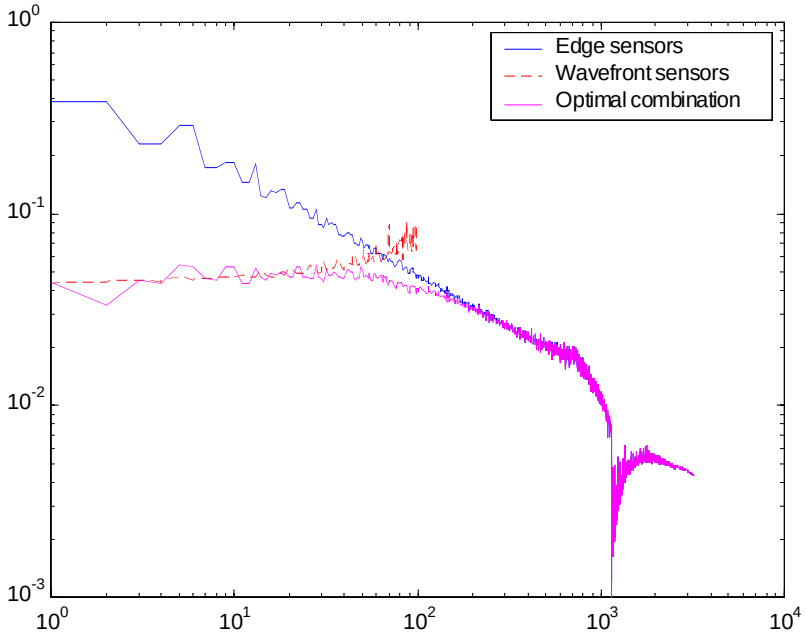

Figure 4. Modal error multiplier for seeing-limited case, in mas of segment rotation per nm of edge sensor noise, comparing edge sensors, wavefront information, and optimal combination. Note that the scale factor between wavefront and edge sensors is arbitrary, for qualitative illustrative purposes only.

[1] Mast, T. and Nelson, J., CELT Telescope Error Budgets , CELT report #10.
[2] Chanan, G., Nelson, J., Ohara, C., and Sirko, E. Design Issues for the Active Control System of the California Extremely Large Telescope (CELT) , SPIE **4004**, 2000.
[3] MacMartin, D.G., Mast, T.S., Chanan, G., and Nelson, J.E., Active Control Issues for the California Extremely Large Telescope , AIAA 2001-4035, 2001.
[4] Mast, T. and Nelson, J. Segmented Mirror Control System Hardware for CELT , SPIE **4003**, 2000.
[5] MacMartin, D.G. Analysis of Gemini Wind Data for CELT (in preparation).
[6] Mast, T.S. and Nelson, J.E., Quarterly Report #1, (Sept 1 - Nov 30, 2000) , CELT Report #12.